

The relationship between inter-annual and intra-annual variability in atmospheric angular momentum in a GCM with climatological SSTs

By STEVEN B. FELDSTEIN, *Cooperative Institute for Research in the Environmental Sciences, University of Colorado, Boulder, CO 80309, USA*

(Manuscript received 17 May 1993; in final form 18 May 1994)

ABSTRACT

The internally generated interannual variability in absolute angular momentum is examined with a 100-year run of a GFDL GCM. Interannual forcing of the atmosphere by the ocean is suppressed as the GCM's sea surface temperatures are constrained to undergo the same annual cycle each year. The interannual variation in the model's globally integrated and annually averaged absolute angular momentum (GAAM) is found to be a moderately large fraction of the changes in the GAAM observed in the atmosphere. The meridional structure of the absolute angular momentum is examined with an EOF analysis. Three modes are found; a tropical mode that represents a strengthening and weakening of the tropical easterlies, and two extratropical dipole modes, one in either hemisphere, that represent latitudinal shifts of the jet maxima. It is shown that the interannual variability of all three modes can be interpreted as resulting from climate noise. The absolute angular momentum budget of all three modes is examined. It is found that the tropical mode depends upon a complex three way balance between the friction and mountain torques and the absolute angular momentum flux convergence, whereas the two midlatitude modes are primarily determined by the absolute angular momentum flux convergence. Fluctuations of the tropical mode are shown to be related to the GCM's Madden-Julian Oscillation, and the midlatitude dipole modes are found to show characteristics in common with the zonal index observed in the atmosphere.

1. Introduction

Most interannual variability in the atmospheric general circulation is generally believed to be related to its coupling with the ocean. As an example, the interannual variation of both the globally integrated absolute angular momentum (GAAM) and the length of day (LOD) have been shown to be highly correlated with the El Niño/Southern Oscillation (see Chao, 1984; Eubanks et al., 1985; Hide and Dickey, 1991). However, internal processes may also play an important role in interannual variability. In order to examine internally generated variability, James and James (1989) used a multi-level primitive equation model with a zonally homogeneous lower boundary and simple linear thermal forcing and frictional

damping. Their results show that the power spectra of the planetary scale vorticity and temperature spectral coefficients resemble a red noise spectrum with variability on decadal time scales. However, they found no statistically significant peaks on these decadal time scales.

In order to further address the role of internal processes for atmospheric interannual variability, we will investigate the interannual variability in a 100-year run of a Geophysical Fluid Dynamics Laboratory (GFDL) general circulation model (GCM) experiment. This GCM includes a full radiation package with predicted clouds, surface hydrology, a moist convective adjustment, and sea surface temperatures (SSTs) which are specified to undergo the same annual cycle each year. Therefore, except for the effect of the model's

surface hydrology, which was found to be small (an examination of the power spectra of some of the model's surface moisture fields showed little power on interannual time scales with no strong spectral peaks), the forcing of the atmosphere on interannual time scales is suppressed and all interannual variability within the model atmosphere is internally generated. We study the model's interannual variability by examining the mechanisms which drive interannual absolute angular momentum changes in different parts of the atmosphere. Absolute angular momentum is the quantity chosen for this purpose since its conservation laws are relatively simple.

As we will see, the interannual variation of the model's absolute angular momentum can be interpreted as arising from processes which take place on intra-annual (less than one year) time scales. Then, there are at least two problems that should be addressed in order to understand the internally generated interannual variability in the model; first the intra-annual variability itself, second, the mechanism by which these short time scale fluctuations determine the longer time scale interannual variability. In this paper, we will focus on the first problem. Therefore, there will be an emphasis toward trying to understand the GCM's absolute angular momentum fluctuations on time scales shorter than one year.

Previous studies have found both interannual and intra-annual variation in absolute and relative angular momentum occurring within the tropics. On interannual time scales, the observational results of Dickey et al. (1992) indicate that the strength of the tropical relative angular momentum fluctuates on time scales from 18 to 88 months and propagates toward high latitudes in both hemispheres. Furthermore, a large covariance between tropical relative angular momentum and GAAM was shown by Rosen et al. (1991) to take place on interannual time scales. For intra-annual times scales, Benedict and Haney (1988), Lau et al. (1989), and Rosen et al. (1991) show that most of the observed relative angular momentum variation is associated with fluctuations in the tropical zonally-averaged zonal winds. Similar results have been found by Boer (1990) with data from the Canadian Climate Centre GCM, and by Robinson (1993) who used an idealized two-level primitive equation model with a homogeneous lower boundary. In addition, Anderson and Rosen

(1983) showed that the observed 40–50 day relative angular momentum is transported both poleward and downward from the upper tropical troposphere. Furthermore, studies such as those by Gutzler and Ponte (1990) and Weickmann et al. (1993) show that fluctuations in tropical relative angular momentum may be associated with the 30–60 day Madden–Julian Oscillation (see Madden and Julian, 1971, 1972).

Both interannual and intra-annual variation in relative angular momentum have also been observed in midlatitudes of both hemispheres. With an 18–35 month filter, Dickey et al. (1992) show dipole structures in the observed midlatitude anomalous relative angular momentum field. These dipoles are characterized by an increase in relative angular momentum at one latitude and a nearby decrease in relative angular momentum at another latitude. In addition, using Empirical Orthogonal Functions (EOFs), James and James (1992) find similar midlatitude structures in their multi-level primitive equation model. An examination of the power spectrum of the principal component time series of this EOF indicates variability on time scales from days to decades. Observational studies that find variability on intra-annual time scales in the midlatitude relative angular momentum are Rosen and Salstein (1983), Lau et al. (1989), Dickey et al. (1991), and Gutzler and Madden (1993). These studies emphasize intra-seasonal relative angular momentum fluctuations. The modeling study of Robinson (1991) found a midlatitude dipole structure in the zonally-averaged zonal wind that fluctuated on intra-annual time scales. This midlatitude structure corresponds to latitudinal displacements of the midlatitude zonally-averaged jet.

The above results indicate that tropical and midlatitude absolute angular momentum variability are characterized by different physical processes. Therefore, it is essential to examine regional variability in absolute angular momentum since GAAM cannot distinguish between tropical and midlatitude variability. For this purpose, we isolate absolute angular momentum in different regions of the atmosphere with an EOF analysis.

The data to be used in this study is presented in Section 2, and a description of the temporal evolution of the GAAM is shown in Section 3. The modal properties of the absolute angular momentum is examined in Section 4 with the aid

of an EOF analysis, and the absolute angular momentum budget of these modes is presented in Section 5. The relationship between these modes and both the model's Madden-Julian Oscillation and low frequency anomalies such as the North Atlantic and North Pacific Oscillations is discussed in Section 6. The Conclusions are presented in Section 7.

2. Data

The data analyzed in this study were generated in a 100 year run of a GFDL GCM. The model has an R15 horizontal resolution, 9 vertical sigma levels, with realistic continents and topography (see Gordon and Stern, 1982 for a description of the model). As mentioned in the introduction, the model's SSTs and solar heating are constrained to follow the same climatological annual cycle each year.

The equation for the conservation of absolute angular momentum in a band of unit meridional width is

$$\begin{aligned} & \frac{\partial}{\partial t} \int_0^{2\pi} \int_0^1 \frac{p_s \mu}{g} a \cos \theta \, d\sigma \, d\lambda \\ &= \frac{-1}{\cos \theta} \int_0^{2\pi} \int_0^1 \frac{\partial}{\partial \theta} \left(\frac{p_s \mu v \cos \theta}{g} \right) \cos \theta \, d\sigma \, d\lambda \\ & - a \cos \theta \left(\int_0^{2\pi} \tau_\lambda a \cos \theta \, d\lambda + \int_0^{2\pi} p_s \frac{\partial h}{\partial \lambda} \, d\lambda \right). \end{aligned} \quad (2.1)$$

This equation relates the angular momentum tendency to the absolute angular momentum flux convergence and the friction and mountain torques. The absolute angular momentum is $\mu = (\Omega a \cos \theta + u) a \cos \theta$, p_s is the surface pressure, u and v are the zonal and meridional winds respectively, g is the gravitational acceleration, a is the earth's radius, τ_λ is the surface wind stress in the zonal direction, and h is the height of the topography. The zonal and meridional length coordinates are λ and θ , respectively. It should be noted that there is also a small torque due to horizontal diffusion of vorticity and divergence in the GCM (this torque is not included in eq. (2.1)). However, this term was found to be negligible compared to the friction and mountain torques.

The surface wind stress from this GCM experiment is saved as monthly averages over every time step. For the zonal and meridional winds and surface pressure, the data are saved at the end of each day. As a result, there must be some sampling error in both the mountain torque and the absolute angular momentum flux convergence, while there is no sampling error in the monthly averaged friction torque. Furthermore, it should be noted that the GCM's equations do not precisely conserve absolute angular momentum. Nevertheless, as we will see, a well balanced angular momentum budget is obtained at most latitudes.

3. Temporal evolution of GAAM

In order to determine whether the amplitude of the GCM's internally generated interannual signal is moderately large compared with observations in the atmosphere, the time series for the anomalous annual GAAM (the difference between each annual average GAAM and the 100 year average GAAM) is examined (see Fig. 1). The GAAM is seen to undergo irregular fluctuations from one year to the next throughout the 100-year time period. In analyzing this time series, a small linear trend was removed. This linear trend was due to a 0.7 mb increase in the horizontally averaged surface pressure during the one hundred years. The source of this trend has been found to be due to round-off error in the surface pressure tendency equation (R. Stauffer, personal communication). If this trend is retained, the results of this study are found to be unchanged. We can convert the year to year changes in the GAAM in Fig. 1 to changes in the LOD using the earth/atmosphere angular momentum conservation relationship in Rosen and Salstein (1983), $\Delta \text{LOD} = 1.68 \times 10^{-26} \Delta \text{GAAM}$, where ΔLOD is the change in the length of day measured in ms and ΔGAAM the change in GAAM. It can be seen that the typical interannual change in the LOD is about 0.1 ms. For a comparison, the observed interannual change in the LOD is typically about 0.35 ms (see Fig. 9 of Hide and Dickey (1991)). Thus, compared with observations, moderately large interannual changes in GAAM or LOD occur even when the boundary forcing (SSTs) is constrained to follow the same annual cycle each year. Assuming that the GCM's variability behaves like that of the

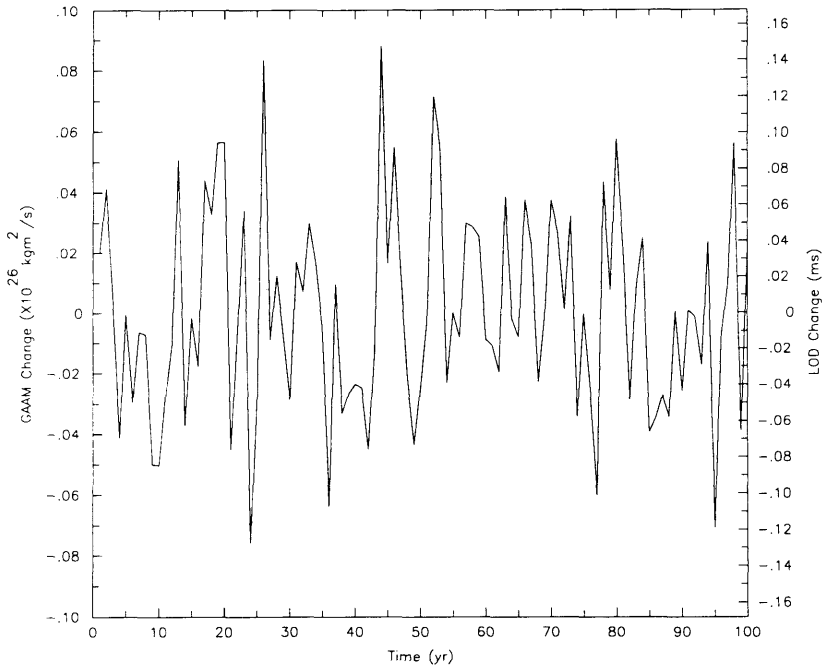


Fig. 1. Time series of anomalous annual GAAM (deviation from 100-year mean) and annual average change in LOD.

atmosphere, the above result indicates that a sizeable internal production of GAAM variation occurs on interannual time scales in the model.

4. Eigenvector analysis

4.1. Characteristics of the EOFs

The meridional structure of the absolute angular momentum is examined with an EOF analysis (for a discussion on EOF analysis see Kutzbach, 1967). In order to perform this calculation, the annual cycle is removed by setting the first three harmonics of the annual cycle equal to zero. The absolute angular momentum is vertically and zonally integrated into 40 separate latitudinal bands, each band having an equal width of 4.5° latitude. The resulting first three EOFs for the monthly averaged absolute angular momentum anomalies (the monthly averaged absolute angular momentum for each band minus the 100 year average absolute angular momentum for that band) are shown in Fig. 2. The first EOF (EOF1), which is mainly of one sign and is concentrated in

the tropics, comprises 24% of the variance. The second and third EOFs (EOF2 and EOF3) make up 18% and 17% of the variance, respectively, and are mostly restricted to midlatitudes of either hemisphere. Furthermore, EOF2 and EOF3 both have a very similar dipole meridional structure. These three modes will also be referred to as the Tropical, Southern Hemispheric (SH), and Northern Hemispheric (NH) modes, respectively. A similar EOF analysis was performed using annual and pentad absolute angular momentum anomalies. For both of these analyses, the structure of the first three EOFs very closely resembles those found from the monthly anomalies.

The role of the three EOFs can be better visualized by adding and subtracting the relative angular momentum EOFs to and from the time mean relative angular momentum field (not shown). (Note that the first three relative angular momentum EOFs were found to be extremely similar to the three absolute angular momentum EOFs shown in Fig. 2.) It was found that the Tropical mode represents oscillations in the strength of the vertically integrated easterly winds

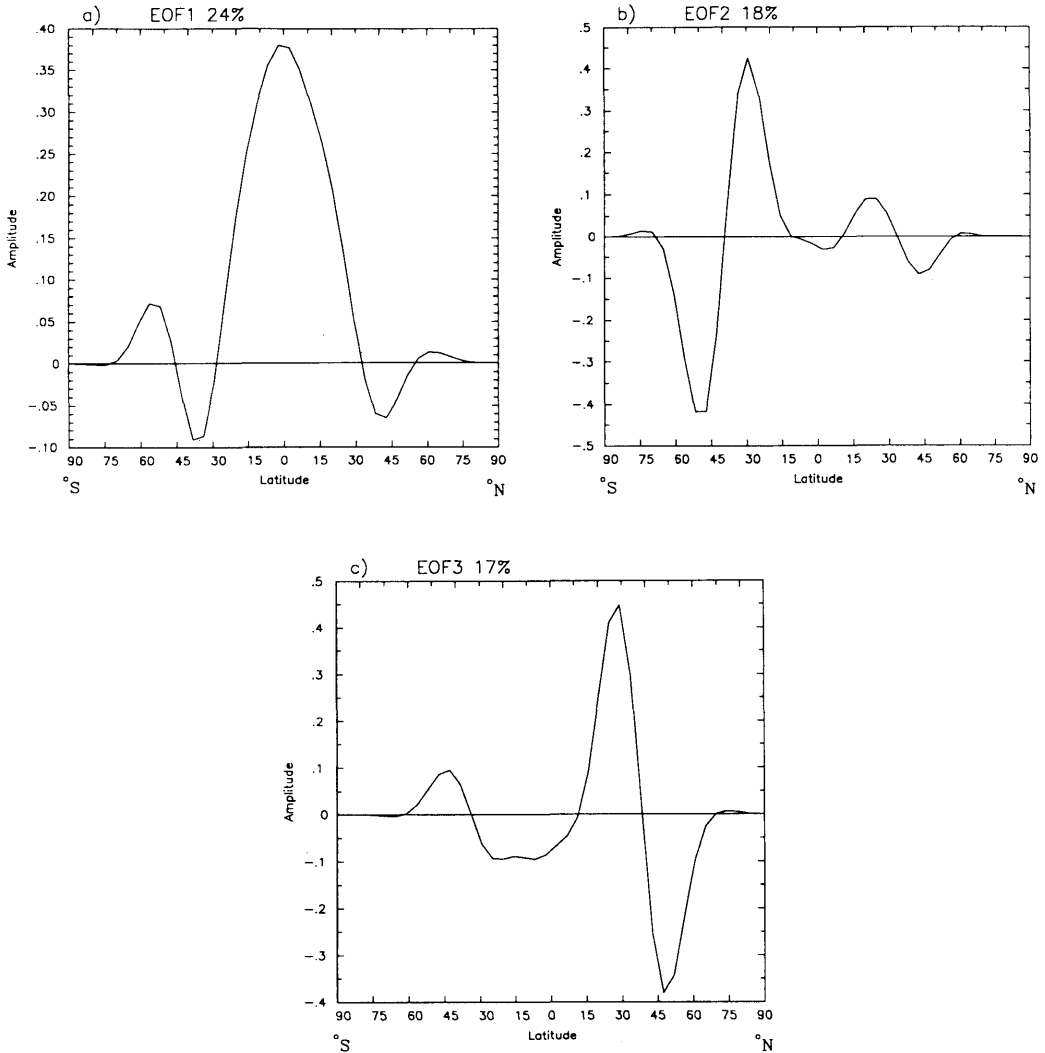


Fig. 2. Meridional structure of the first three absolute angular momentum EOFs. The monthly averaged absolute angular momentum is used to generate these EOFs.

in the tropics. Also, during a small number of months, when the amplitude of the Tropical mode is sufficiently positive, it was found that the vertically integrated winds in the tropics became westerly. The two extratropical modes, on the other hand, were found to correspond to independent meridional displacements in the latitude of the jet maximum of either hemisphere.

We next examine the linear correlation between the GAAM time series and the principal com-

ponents of the three modes, which are related by the expression

$$GAAM(t_l) = \sum_{j=1}^N c_j(t_l) \sum_{i=1}^M e_j(y_i) \Delta y_i. \quad (4.1)$$

This expression is derived by noting both that

$$GAAM(t_l) = \sum_{i=1}^M AAM(y_i, t_l) \Delta y_i,$$

where

$$\text{AAM}(y_i, t_i) = \sum_{j=1}^N c_j(t_i) e_j(y_i)$$

denotes the absolute angular momentum in the i th latitude band at time t_i , $c_j(t_i)$ the coefficient of the j th EOF at time t_i (this coefficient is referred to as the j th principal component), $e_j(y_i)$ the j th EOF evaluated at the i th latitude band, N the number of EOFs, M the number of latitude bands, and Δy_i the latitudinal extent of each band. The linear correlation between the GAAM time series and the principal component time series of EOF1, EOF2, and EOF3 is found to be 0.89, 0.06, and -0.14 , respectively. This small correlation between the time series of the two extratropical modes and the GAAM isn't surprising because the latitudinal integration of these modes has a large amount of cancellation. The large linear correlation between the principal component of EOF1 and the GAAM time series do suggest that there is a strong link between the Tropical mode and the GAAM. This relationship between GAAM and tropical absolute angular momentum is consistent with the results of several observational studies as summarized in the introduction.

In order to verify that the above modes correspond to structures observed in the GCM data and do not occur as a result of the constraints associated with the EOF analysis, separate EOF analyses of the monthly averaged absolute angular momentum were performed with the atmosphere divided into three regions; north of 20°N , between 20°N and 20°S , and south of 20°S . These EOF analyses revealed that the first EOF for the region north of 20°N resembled the NH mode, the first EOF in the region between 20°N and 20°S was very similar to the Tropical mode, and the first EOF for the region south of 20°S looked very much like the SH mode. The same behavior was also found for annual and pentad averaged angular momentum. The eigenvalues and associated standard errors (see North et al., 1982) for each EOF are shown in Table 1. It can be seen that all three EOFs are distinct for the monthly and pentad anomalies, but EOF2 and EOF3 for the annual anomalies do not appear to be strongly distinct, as the sum of their standard errors is greater than the difference between their eigenvalues. Nevertheless, the annual averaged

EOF2 and EOF3 are regarded as distinct physical modes since as indicated above, these modes appear in separate EOF analyses of either hemisphere. Even on physical grounds, because there is a fairly large degree of cross-equatorial symmetry in the zonally-averaged climatological flow, it is not surprising to find EOFs in either hemisphere with similar eigenvalues.

The month to month variation of each mode is also examined by counting the number of months during the entire 100-year period for which the principal component of the EOF exceeds a value that is greater or less than one standard deviation from its mean. It was found that the Tropical and SH modes undergo very little seasonal variation whereas the NH mode is strong mostly during winter. These results are also similar to those of Lau et al. (1989) who show that their tropical,

Table 1a. *The eigenvalues ($\times 10^{12}$), % variance, and standard error ($\times 10^{12}$) for annual absolute angular momentum anomalies*

	Eigenvalue (λ)	% variance	Standard error ($\delta\lambda$)
EOF1	1.00	33	0.183
EOF2	0.569	19	0.104
EOF3	0.430	14	0.079

Table 1b. *The eigenvalues ($\times 10^{12}$), % variance, and standard error ($\times 10^{12}$) for monthly absolute angular momentum anomalies*

	Eigenvalue (λ)	% variance	Standard error ($\delta\lambda$)
EOF1	4.80	24	0.200
EOF2	3.72	18	0.154
EOF3	3.30	17	0.137

Table 1c. *The eigenvalues ($\times 10^{12}$), % variance, and standard error ($\times 10^{12}$) for pentad absolute angular momentum anomalies*

	Eigenvalue (λ)	% variance	Standard error ($\delta\lambda$)
EOF1	7.36	19	0.122
EOF2	6.73	17	0.112
EOF3	6.00	15	0.099

tropical/subtropical, and Southern Hemispheric extratropical modes experience little seasonal variation while their Northern Hemispheric extratropical mode is apparent only in winter.

The skewness of the monthly averaged principal components of all three modes is examined by determining the frequency in which the principal component falls within specified intervals. These frequencies are found to be symmetric (not shown) for all three modes which indicates that there is no preference for a particular phase of a mode. This result contrasts that of Robinson (1991), who showed with a primitive equation model with a zonally homogeneous lower boundary that the dominant mode (his dominant mode closely resembles the two extratropical modes of the present study) is strongly skewed toward what would correspond to the positive phase of EOF2 and EOF3.

The presence of any relationship between the tropical and the two extratropical modes is tested with a series of lag cross-correlations between the principal components for all three EOFs. The resulting linear correlations were all negligible, suggesting that all three modes are independent of one another. Analogous behavior was found in a study of low-frequency variability of 700 mb heights by Ghil and Mo (1991a, b). In those studies, modes in the tropics and in both the Northern and Southern Hemisphere were confined to a 10 to 120 day band. As in the present study, the authors found that there were no statistically significant correlations between any of their three modes.

4.2. Climate noise test

The power spectra of the pentad principal component time series for the Tropical, SH, and NH modes are shown in Fig. 3. In this spectrum, the annual cycle is removed by setting the first three harmonics of the annual cycle equal to zero. Then, the power spectrum is smoothed by using a Hanning window with a lag of 10 years. Also shown in Fig. 3 is both a red noise spectrum based on a one pentad lag autocorrelation and the corresponding 5% and 95% significance levels. As can be seen, the SH and NH modes exhibit a red noise spectrum, with a no spectral peaks that exceed the 95% significance level. On the other hand, for the Tropical mode, there are several peaks with periods between 20 and 120 days that exceed the

95% significance level. However, except for the spectral peak centred near 45 days in Fig. 3a, which overlaps with the 40–50 day spectral peak in atmospheric angular momentum observed in the atmosphere, there are no a priori reasons to expect that any of the other spectral peaks associated with the Tropical mode are statistically significant.

Because of the similarity in the structure of the EOFs for pentad, monthly, and annual anomalies, we anticipate that there is also a corresponding relationship between the pentad, monthly, and annual principal components for each EOF. In order to analytically derive this relationship between the principal components, it is assumed for simplicity that the EOFs from annual and pentad averaged data are identical (the validity of this assumption for the angular momentum data will be verified later). Consider the absolute angular momentum anomaly matrix x_{il} for the pentad time series, where the subscript i denotes the latitude and l the time. If x_{il} is decomposed into EOFs, the relationship $x_{il} = \sum_j e_{ij} c_{jl}$ is satisfied, where e_{ij} is the matrix of EOFs and c_{jl} the matrix of principal components. The first subscript of e_{ij} (c_{jl}) denotes the latitude (the particular EOF) and the second subscript indicates the particular EOF (time). Following the assumption that the e_{ij} are the same for both the pentad and annual time series, by summing every individual element x_{il} and c_{jl} separately for each year, one finds that $X_{ik} = \sum_j e_{ij} C_{jk}$, where

$$X_{ik} = \frac{1}{N} \sum_{l=a}^b x_{il}, \quad C_{ik} = \frac{1}{N} \sum_{l=a}^b c_{il}; \quad (4.2)$$

$N = 73$, which is the number of pentads in a single year, $a = N(k - 1) + 1$, $b = Nk$, and the matrix X_{ik} is just the absolute angular momentum anomaly matrix with annual averaged data. This relationship in (4.2) indicates that if the structure of the EOFs is the same for data based on either annual or pentad averages, then the principal components calculated from annual averaged data, C_{ik} , must be equal to the mean of the principal components generated from pentad data where this mean is calculated separately for each year. In order to examine the extent to which this relationship holds in the present study, the following procedure is adopted. First, the principal components for the EOFs from the pentad anomaly time series are summed separately for each year. This gives a

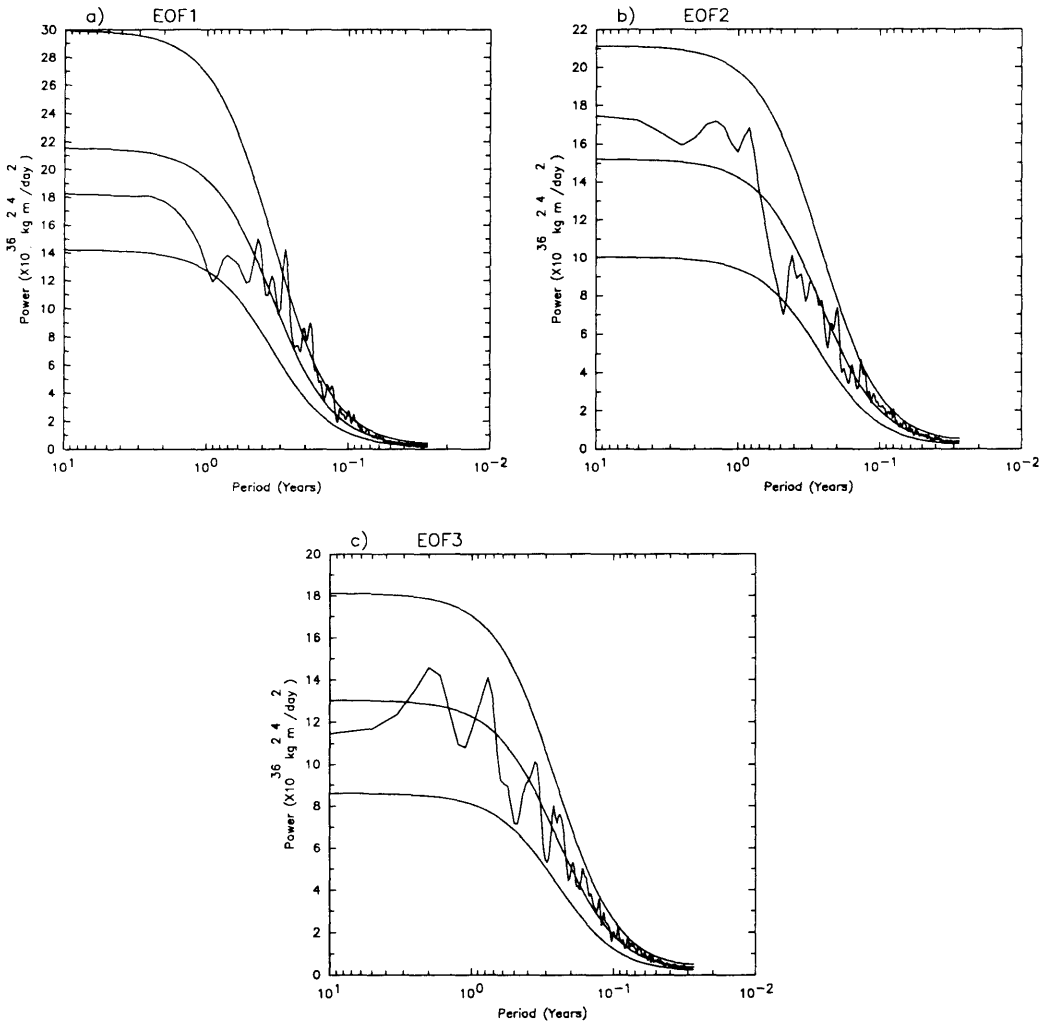


Fig. 3. Power spectra of the principal components for the first three absolute angular momentum EOFs. This is compared with its red noise spectrum and corresponding 5% and 95% significance levels (note that the area under the curve is not proportional to the variance).

times series consisting of 100 values. Then, a linear correlation is performed between the time series of yearly data constructed from this pentad anomaly time series with the time series consisting of the principal components of the EOFs from the annual anomaly time series. This linear correlation is calculated separately for all three modes. The resulting linear correlation for the Tropical mode is 0.95, for the SH mode 0.85, and for the NH mode 0.91. Similar results are obtained if a time series is

constructed from the principal components of the monthly anomaly times series.

Because of the above relationship amongst the EOFs and principal components, we next address the question whether the interannual variation of all three modes is due to processes that involve the same mode which occur on time scales much less than one year. Stated in other words, whether the variation of the annual-averaged principal components results from statistical sampling fluctua-

tions because of contributions from unpredictable shorter time scale events toward the annual time average. This is often referred to as "natural variability" or "climate noise" (Leith, 1973; Madden 1976, 1981; Madden and Shea, 1978). Therefore, we address the question whether "climate noise" is sufficient to account for the interannual variability in the principal components. In order to examine this question, following the procedure in Trenberth (1984), we calculate the ratio $F = \sigma_m^2 / \sigma_n^2$, where σ_m^2 is the interannual variance of the annual averaged pentad time series, and σ_n^2 is the interannual variance of an annual averaged time series modeled by a first-order Markov process. For the calculation of σ_n^2 , the lag one autocorrelation of the pentad principal component time series is used (see Madden, 1981). We specify a null hypothesis that $F = 1$, and then examine the statistical significance of F for all three modes. As shown in Trenberth (1984), the above ratio should follow the F distribution with $J - 1$ degrees of freedom for the numerator and $J(N_{\text{eff}} - 1)$ degrees of freedom for the denominator, where $J = 100$ is the number of years in the time series, $N_{\text{eff}} = N/T_0$, with T_0 being the time between independent pentad samples, and $N = 73$ is the number of pentads in a year. Since T_0 was found to be similar for all three modes, with values close to 7 pentads, the critical value of F at the 95% significance level is approximately the same for each mode with a value of 1.28. The values of F were calculated and found to be 0.98, 1.04, and 0.97, for EOF1, EOF2, and EOF3, respectively. Therefore, the null hypothesis is accepted and the interannual variation of all three modes is interpreted as arising from climate noise.

The question of whether a "potentially predictable" climatic signal could be distinguished from climate noise was examined by Zwiers (1987) in a GCM with climatological SSTs (see Trenberth, 1985 for an example of the examination of the potential predictability of the atmosphere). Unlike the present study, where no potential predictability on interannual time scales is found, he did find potential predictability both in the tropics and in high latitudes. However, the variables examined were surface pressure and 500 mb height, not angular momentum. The absence of potential predictability in the principal components of EOF2 and EOF3 is consistent with the results of Zwiers (1987), since as mentioned above, he does

not find potential predictability in the midlatitudes of both hemispheres. However, the lack of potential predictability in the principal component of EOF1, which is the mode with largest amplitude in the tropics, clearly does not follow the results of Zwiers (1987). These differences in potential predictability can most likely be explained by considering the surface pressure field. The first surface pressure EOF of Zwiers (1987) is a pattern that represents a transfer of mass between high and low latitudes. He found strong interannual variability for this mode. In the present study, the first surface pressure EOF does not show this pattern, but instead indicates a mass transfer between middle and high latitudes. This EOF pattern closely resembles that found in the observational study of Trenberth and Christy (1985).

It is important to state that when one examines annual averages of a time series described by a red noise process that the time averaging filters out most of the power on intra-annual time scales. However, on this time scale, most processes in the atmosphere and in the GCM take the form of "pulses". That is, there is a growth phase, followed by maintenance of the anomaly for some period of time, and then the decay phase. For example, the complete life cycle of synoptic-scale baroclinic waves typically takes several days. In extreme cases, such as explosive cyclogenesis, the cycle may last only one day. Other well known examples take place on intraseasonal time scales. These include midlatitude low frequency anomalies, such as the Pacific/North America pattern (e.g., Wallace and Gutzler, 1981) and the tropical anomaly pattern associated with the Madden-Julian Oscillation (MJO, see Madden and Julian, 1971, 1972). Furthermore, the period of these "pulses" is very irregular, as is their occurrence and their amplitude. Because of the above properties, a Fourier transform of these "pulses" will include periods at time scales greater than one year, and it is these periods that are retained in an annual-average time series. (As discussed by Mitchell (1976), the effect of short time scale processes on a power spectrum is simply to add white noise to the power spectrum on all time scales substantially longer than that of the process. Thus, no matter how short the time scale, there will always be a white noise contribution to the power spectrum on inter-annual time scales.) Since the principal components of all three EOFs also behave as "pulses",

we are interpreting the annual-average time series of their principal components as representing the very low-frequency component of highly irregular, unpredictable processes which take place on intra-annual time scales. Such an interpretation of inter-annual variability, which follows the definition of climate noise, is understandable for the present GCM, because the climatological SST specification implies an absence of forcing of the model's atmosphere on interannual time scales. Therefore, we can interpret the interannual variation of all three modes as arising from climate noise. As a result, we will shift our focus toward understanding fluctuations of absolute angular momentum which take place on time scales shorter than one year.

5. Angular momentum budget

We next use monthly averaged data to determine the composite absolute angular momentum budget for all three modes. Monthly averaged data is used for this budget, instead of pentad data which would be preferable, because the surface stresses from the GCM run are saved as monthly averages. In order to try to compare budgets with pentad and monthly averaged data, a pentad budget was analyzed with the surface stresses represented by the GCM's bulk parameterization scheme. The resulting budget was found to be very similar to that which we will see with monthly averaged data. The procedure for computing the budget is started by calculating the EOFs of the monthly averaged absolute angular momentum tendency. These EOFs (not illustrated) have the same structure as those shown earlier for the absolute angular momentum. Then, composites of anomalous absolute angular momentum tendency, absolute angular momentum flux convergence, friction and mountain torques are determined from those months during which the principal components of the absolute angular momentum tendency EOFs exceed or are less than one standard deviation from their mean. This procedure generates two sets of months that will be referred to as the positive and negative phases of a particular EOF. The above criteria is satisfied for 193 months for the positive phase and 184 months for the negative phase of EOF1, 202 and 184 months for the positive and negative phases of

EOF2, and 178 and 187 months for the positive and negative phases of EOF3.

In this study, the absolute angular momentum budget will be displayed as the difference between composites for the positive phase of the EOF minus the composites for the negative phase of the EOF, since the two phases always exhibit similar patterns but of opposite sign. The extent to which the budget is balanced can be seen in Fig. 4 where the anomalous absolute angular momentum tendency and the sum of both anomalous torques and the anomalous absolute angular momentum flux convergence are compared. The similarity in the sets of curves in Fig. 4 shows that the budget for all three modes is indeed well balanced, especially at latitudes where the EOF has a large amplitude.

The separate terms that comprise the angular momentum budget are shown in Fig. 5. For the Tropical mode (see Fig. 5a), there is a complex three way balance between the anomalous absolute angular momentum flux convergence and the anomalous friction and mountain torques. In midlatitudes, where the amplitude of the mode is relatively small, the sum of the two anomalous torques tends to have opposite sign from the anomalous absolute angular momentum flux convergence. On the other hand, in the tropics, where the mode has its largest amplitude, the anomalous absolute angular momentum flux convergence and anomalous friction torque reinforce one another. The anomalous absolute angular momentum flux convergence dominates within a band of about ten degrees latitude on either side of the equator whereas the anomalous friction torque dominates in the subtropics. This structure for the anomalous friction torques is consistent with that of the idealized Gill model (see Gill, 1980), where the zonally-averaged low level easterlies are strongest on either side of the equator, and not along the equator. Furthermore, by examining the terms that comprise the anomalous absolute angular momentum flux convergence, i.e., the eddy, meridional, and omega angular momentum flux convergences (for a definition of these terms, see Holton, 1992, pp. 333-335), it is found that the eddy angular momentum flux convergence dominates the other two terms.

A simple picture involving wave activity propagation may explain some of the properties of the absolute angular momentum budget for the

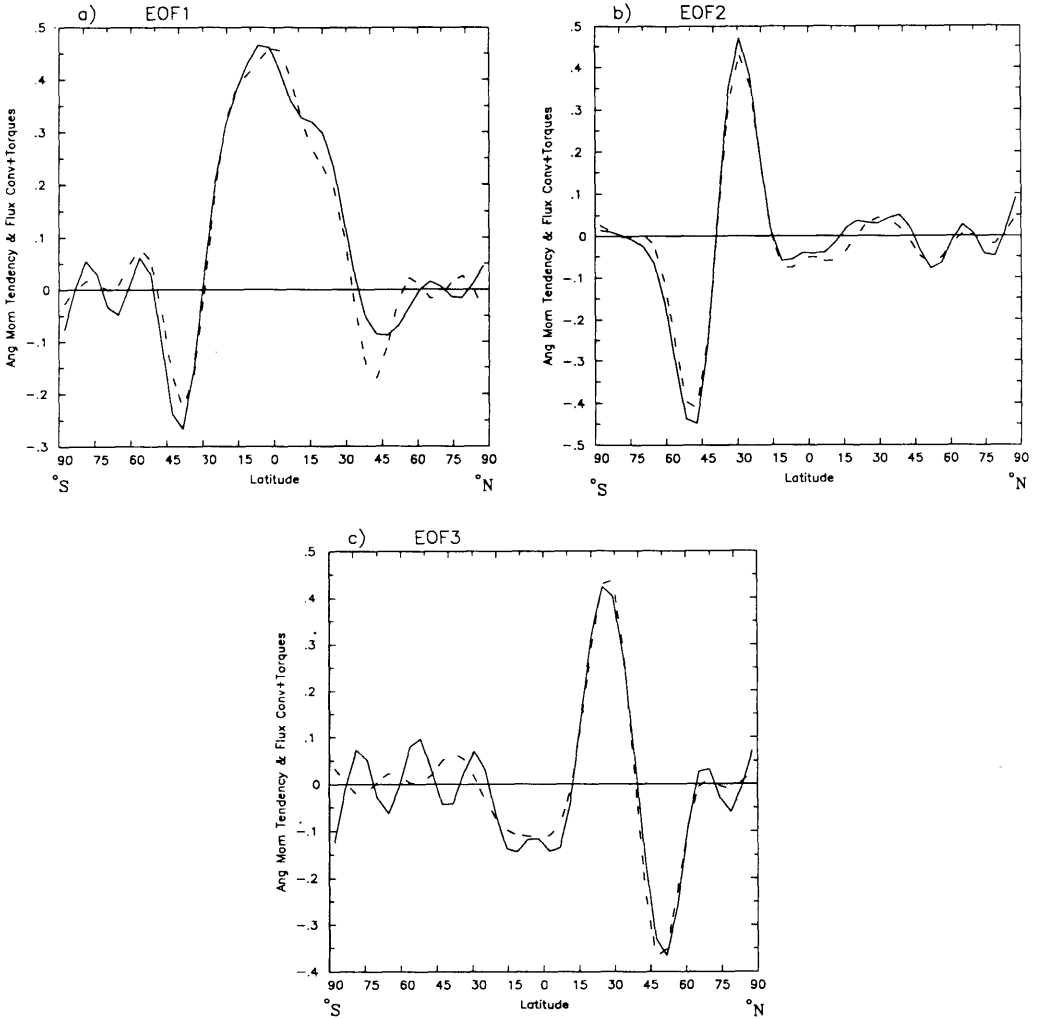


Fig. 4. Composites of anomalous absolute angular momentum tendency (dashed line) and the sum of the anomalous friction and mountain torques and the absolute angular momentum flux convergence (solid line) for the first three absolute angular momentum tendency EOFs (the explanation of the compositing procedure is discussed in the text). Units $\times 10^{18} \text{ kg m}^2 \text{ s}^{-2}$.

tropical mode. Consider the effect of a source of isolated heating due to convection within the tropics. According to the Gill model, the response to this heating includes a zonally symmetric component in the subtropics which is westerly at upper levels and easterly at lower levels. The low level easterlies are then damped by surface friction which results in a positive friction torque and a net gain of absolute angular momentum. At the same

time, the convection also generates a localized region of wave activity in the tropics. As this wave activity propagates toward midlatitudes, the tropical absolute angular momentum must further increase (see Held and Phillipps (1987) for a discussion on wave activity and its affect on the background zonally-averaged flow). Some time later, the wave activity converges in midlatitudes which in turn causes the midlatitude absolute angular

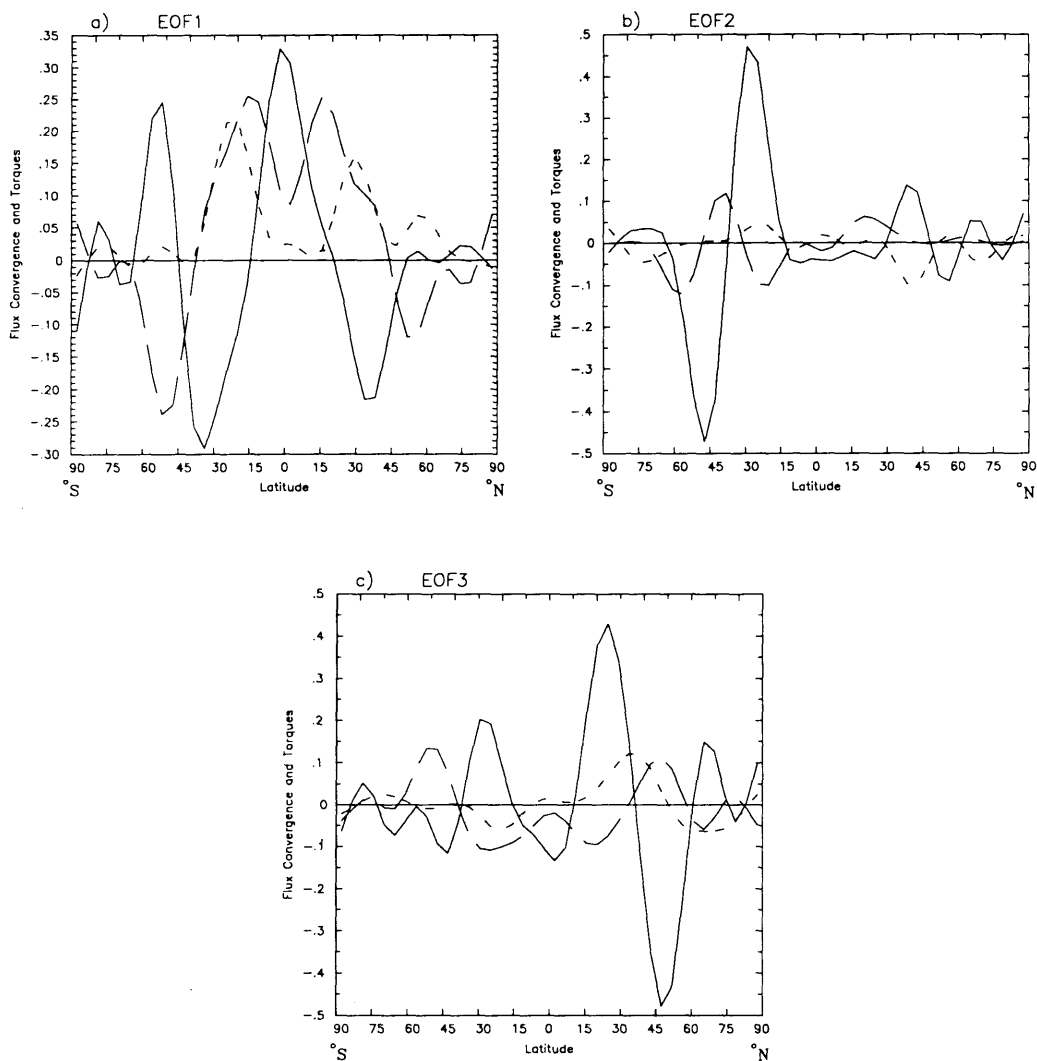


Fig. 5. Composites of anomalous friction torques (long dashed line), anomalous mountain torques (short dashed line), and the anomalous absolute angular momentum flux convergence (solid line) for the first three absolute angular momentum tendency EOFs. Units $\times 10^{18} \text{ kg m}^2 \text{ s}^{-2}$.

momentum to decrease. However, the location of the wave activity is such that the accompanying surface pressure and surface wind anomalies generate mountain and friction torques which approximately balance the anomalous absolute angular momentum flux divergence in midlatitudes.

The Tropical mode is examined more closely with a series of composites of the two-dimensional, monthly averaged, anomalous mountain and fric-

tion torques, and precipitation. This composite procedure is identical to that which was followed for calculating the terms in the absolute angular momentum budget for all three EOFs as shown in Figs. 4, 5. As a result, the same months are selected for the present composites as were used in examining those budgets. For these composites, the annual cycle has been removed at each grid point. The composite anomalous mountain and

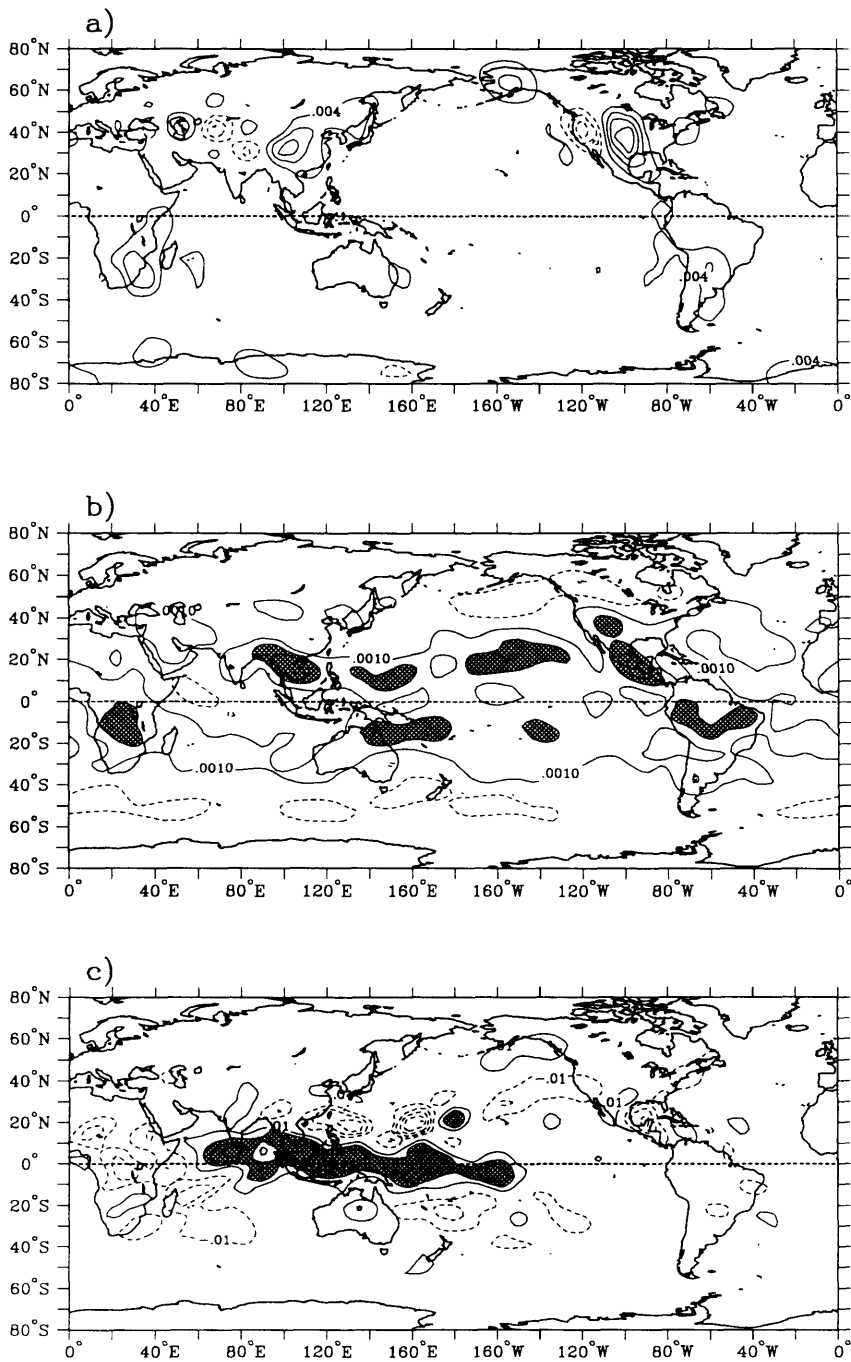


Fig. 6. Composites of (a) anomalous mountain torque, (b) anomalous friction torque, (c) anomalous precipitation for EOF1. Solid contours are positive and dashed contours negative. Contour interval in (a) is $0.01 \text{ kg m}^{-1} \text{ s}^{-2}$, in (b) is $0.002 \text{ kg m}^{-1} \text{ s}^{-2}$, where shading is above $0.003 \text{ kg m}^{-1} \text{ s}^{-2}$, in (c) is 0.01 cm/day , where shading is above 0.03 cm/day . The zero contour is omitted.

friction torques for the Tropical mode are shown in Figs. 6a, b. These anomalous torques are displayed locally as

$$\frac{p_s}{a \cos \theta} \frac{\partial h}{\partial \lambda} \cos^2 \theta \quad \text{and} \quad \tau_\lambda \cos^2 \theta,$$

respectively. The anomalous mountain torque shows large contributions from the Himalayas and Rockies in the Northern Hemisphere, and from the Andes and East African highlands in the Southern Hemisphere. The largest anomalous friction torques come from southeast Asia, the central subtropical Pacific Ocean, and Mexico in the Northern Hemisphere, and from southeast Africa, the subtropical western Pacific Ocean, and central South America in the Southern Hemisphere. The location of the positive anomalous precipitation associated with the Tropical Mode (see Fig. 6c) is largest in the Indian and western Pacific Ocean and is confined to the vicinity of the equator. This location is consistent with the picture presented earlier in this section where a possible relationship between a tropical heating anomaly and the various terms in the absolute angular momentum budget was suggested.

The extratropical modes exhibit a very different balance than that for the Tropical mode (see Figs. 5b, c). For both extratropical modes, it is basically the absolute angular momentum flux convergence alone that drives the fluctuation of these modes as the friction and mountain torques are substantially smaller. Furthermore, as previously stated for the Tropical mode, it was found that the absolute angular momentum flux convergence is dominated by the eddies.

The sensitivity of each of the above composite calculations to the particular threshold value was also examined. This was accomplished by re-calculating the composites with 0.5, 1.5, and 2.0 standard deviation thresholds and comparing the results to that for the one standard deviation threshold which was used throughout this section. It was found that as the threshold value was lowered, all the terms shown in Figs. 4–6 decreased in amplitude, as expected, but the pattern remained essentially the same. This indicates that the above characteristics of the angular momentum budget for all three EOFs is not sensitive to the threshold value chosen.

6. Discussion

6.1. Tropical mode

One dominant feature that appears in observations of the tropics is the MJO. There have been many observational studies of the MJO. These include those by Lau and Chan (1985), Weickmann et al. (1985), Lau and Phillips (1986), and Knutson and Weickmann (1987). The MJO was also found in a GFDL GCM by Lau and Lau (1986) and in an aqua-planet GCM by Hayashi and Sumi (1986). A relationship between the MJO and changes in the relative angular momentum has been investigated by Madden (1987, 1988). He suggested that the tropical friction torque associated with the strengthening of the easterlies to the east of convection, as the convection moves from the tropical Indian to Pacific Ocean, could account for the 30–60 day oscillation in absolute angular momentum. Results consistent with Madden's theory were found by Kang and Lau (1990) for the Northern Hemisphere summer. Weickmann et al. (1993) examined the variation of relative angular momentum associated with the MJO and found similar results with both Madden (1987, 1988) and Kang and Lau (1990) for the Northern Hemisphere summer, but during the Northern Hemisphere winter, they found that the mountain torques are also important for the angular momentum balance.

Because the above observational studies suggest that there may be a relationship between the GAAM and the MJO in the atmosphere, we address the question whether there is a relationship between the MJO in the model and the Tropical mode. The MJO is first defined by performing an EOF analysis on the $\sigma = 0.830$ level velocity potential. The velocity potential is chosen to define the MJO as in Lorenc (1984), Lau and Lau (1986), Knutson and Weickmann (1987), and von Storch and Xu (1990). For this calculation, the annual cycle is removed and the velocity potential is restricted to a latitude band between 30°S and 30°N . The first two EOFs for the $\sigma = 0.830$ velocity potential are shown in Fig. 7. These EOFs are calculated from a pentad anomaly time series at each grid point. As is found in both Lau and Lau (1986), and Knutson and Weickmann (1987), the first two EOFs are in quadrature. Similar patterns to these two EOFs were found by von Storch and Xu (1990) for the first two POP (Principal

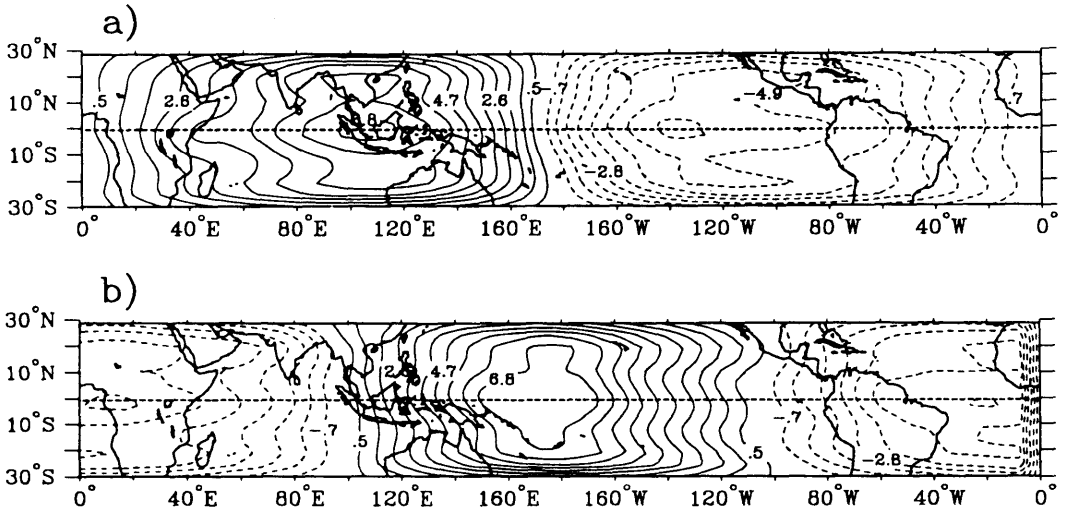


Fig. 7. Horizontal structure of the first two $\sigma = 0.83$ velocity potential EOFs. Contour interval 0.7; contour labels are multiplied by 10^2 . The zero contour is omitted.

Oscillation Pattern) associated correlation patterns. Furthermore, as also found by Lau and Lau (1986) for an R15 GFDL GCM, the power spectra (not shown) for the principal components of the EOFs show a broad statistically significant spectral peak from 25 to 40 days. These spectral peaks in the model's MJO overlap with the 20–120 day spectral peaks in the principal component of the Tropical mode.

In order to examine the above conjecture that the model's MJO is related to the Tropical mode, the principal components of the first two velocity potential EOFs are first used to generate a set of composites of the absolute angular momentum tendency. In a manner similar to that in the previous section, the composites are derived from pentads during which the principal component is one standard deviation either above or below their mean. Since the composite absolute angular momentum tendency is found to keep its meridional structure but undergo a sign change for either phase of both EOFs, the composites are displayed as the difference between the absolute angular momentum tendency during the positive and negative phases of the first two velocity potential EOFs (see Fig. 8). From these composites, it can be seen that these angular momentum tendencies are confined to the tropics and their structure and amplitude resemble that of the Tropical mode.

6.2. Extratropical modes

As was illustrated in the previous section, the two extratropical modes indicate a dipole meridional structure in the absolute angular momentum field. This dipole structure corresponds to a north/south latitudinal displacement of the jet. Similar dipole structures in the zonally-averaged zonal

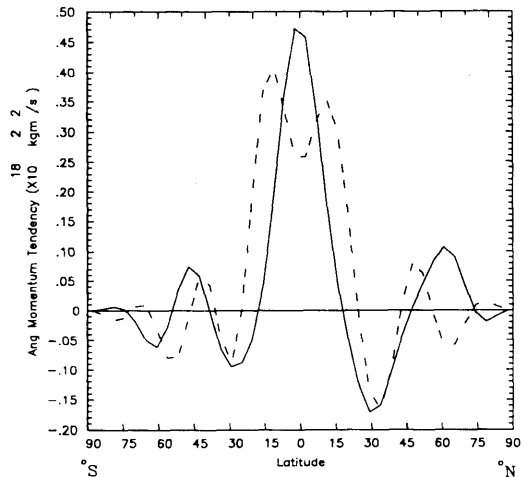


Fig. 8. Composites of anomalous absolute angular momentum tendency for $\sigma = 0.83$ velocity potential EOF1 (solid line) and EOF2 (dashed line).

wind of the Southern Hemisphere have been seen by Trenberth (1979) and Kidson (1986, 1988). In the Northern Hemisphere, Wallace and Hsu (1985) find similar dipole patterns in the 500 mb height field. These patterns were composites based on the zonal index that was introduced by Rossby (1939), defined as the difference in surface pressure between 35°N and 55°N. During the high (low) phase of the zonal index, the Northern Hemisphere jet is displaced northward (southward).

We suggest that the NH mode is a zonal average of the first two EOFs in Ting and Lau (1993) (see Fig. 2 of their paper); using the same 100-year GCM dataset, they examined the low-frequency anomalies of 515 mb geopotential height during the Northern Hemispheric winter (defined as from November to March). The authors relate the first two EOFs to patterns such as the North Atlantic and North Pacific Oscillations as described by Walker and Bliss (1932), Van Loon and Rogers (1978), and Wallace and Gutzler (1981), which exhibit north-south dipoles in both oceans. The extreme values of their anomalous zonal winds occur at 30°N and 50°N for both EOFs which are at the same latitudes where the anomalous absolute angular momentum associated with the NH mode also attains its extreme values.

In order to test the above relationship, composites of anomalous absolute angular momentum are generated that are based on the principal components of the first two EOFs found by Ting and Lau (1993). The months chosen for these composites are those that satisfy a one standard deviation threshold. It was found (not shown) that the absolute angular momentum composites for both EOFs strongly resemble the NH mode of the present study. In order to further test this relationship, composites of anomalous 515 mb geopotential height and wind velocity based on the principal component of the NH mode were generated (not shown). These composites showed the combined patterns of the first two EOFs of Ting and Lau (1993). Furthermore, Ting and Lau (1993) also find that their first two EOFs are maintained by the anomalous vorticity fluxes, consistent with the NH mode being balanced by the anomalous eddy absolute angular momentum flux convergence. Similar results have been found in the observational study of Wallace and Hsu (1985) who found that composites of 500 mb height based on a zonal

index also yield patterns that resemble the North Atlantic and North Pacific Oscillations.

Composites of anomalous 515 mb geopotential height and wind velocity based on the principal component of the SH mode were also made (not shown). These composites revealed patterns with a fairly large degree of zonal symmetry with extreme winds of opposite sign occurring at the same latitude as the extrema in absolute angular momentum for the SH mode. Similar anomalous geopotential height and wind fields that exhibited a large zonally-symmetric component were found by Rogers and Van Loon (1982) and Kidson (1986) in studies of low-frequency zonal flow variability in the Southern Hemisphere.

7. Conclusions

The data from a 100-year run of a GFDL GCM with a climatological SST seasonal cycle was used to examine the internal production of the interannual variation of atmospheric absolute angular momentum. The latitudinal structure of these absolute angular momentum variations was determined with an EOF analysis and was seen to consist of three separate modes; a Tropical mode that represents an acceleration and deceleration of the tropical easterlies, and a dipole mode in either hemisphere which indicates latitudinal displacements of the midlatitude jets. Furthermore, a series of linear correlations showed that the vast majority of the variability in the GAAM could be explained by the Tropical mode.

These three modes were found in EOF analyses that were based on annual, monthly, and pentad anomaly time series. By comparing the variance of the principal component time series of each EOF on interannual time scales to that for the annual averages of a times series modeled by a first-order Markov process, we demonstrated that the interannual variability of these modes results from sampling fluctuations, i.e., climate noise.

The angular momentum budgets of all three modes were examined. The Tropical mode was found to be accelerated by both the friction torque and absolute angular momentum flux convergence within the tropics. This mode extends its influence into midlatitudes where there is a cancellation between the sum of the two torques and the absolute angular momentum flux convergence in

either hemisphere. For the midlatitude modes, a much simpler balance was found where the changes in the absolute angular momentum are due primarily to the convergence of the absolute angular momentum flux.

The first two EOFs of the $\sigma = 0.830$ velocity potential were used to define the GCM's MJO. Composites of absolute angular momentum tendency that were based on the principal components of these EOFs showed a close resemblance to the Tropical mode both in structure and amplitude.

Composites of anomalous geopotential height and wind velocity based on the principal components of the SH and NH modes showed strong similarities with the observed zonal index in both hemispheres. Furthermore, these composites revealed similar dipole patterns in either hemisphere, except the composites are largely zonally symmetric in the Southern Hemisphere and restricted to the two oceanic regions in the Northern Hemisphere. This suggests that the same physical processes may be taking place in either hemisphere and that the large amplitude stationary waves in the Northern Hemisphere are concentrating the dipoles into the two oceanic regions. These results also suggest that an under-

standing of the mechanisms that drive the North Atlantic and North Pacific Oscillations might be found with simpler quasi-geostrophic or primitive equation models with a zonally uniform lower boundary. In such models, the onset, persistence, and decay of the midlatitude dipole modes can be studied systematically as model parameters such as the supercriticality of the zonal wind are varied. Such studies are being planned for in future research.

8. Acknowledgements

I would like to thank Drs. Cecile Penland, Klaus Weickmann, Randy Dole, and Sukyoung Lee for their very beneficial discussions and comments on this manuscript. I would also like to thank Drs. Isaac Held, George Kiladis, Clara Deser, and three anonymous reviewers for their helpful comments on this manuscript, and Drs. Roland Madden, Mingfang Ting, and Prashant Sardeshmukh for their valuable discussions. In addition, I would also like to thank Mary Jo Nath for performing the GCM experiment that was analyzed in this study. This work was supported by the NOAA Climate and Global Change Program.

REFERENCES

- Anderson, J. R. and Rosen, R. D. 1983. The latitude-height structure of 40–50 day variations in atmospheric angular momentum. *J. Atmos. Sci.* **40**, 1584–1591.
- Benedict, W. L. and Haney, R. L. 1988. Contribution of tropical winds to subseasonal fluctuations in atmospheric angular momentum and length of day. *J. Geophys. Res.* **93**, 15973–15978.
- Boer, G. J. 1990. Earth-atmosphere exchange of angular momentum simulated in a general circulation model and implications for the length of day. *J. Geophys. Res.* **95**, 5511–5531.
- Chao, B. F. 1984. Interannual length-of-day variation with relation to the Southern Oscillation/El Niño. *Geophys. Res. Lett.* **11**, 541–544.
- Dickey, J. O., Ghil, M. and Marcus, S. L. 1991. Extratropical aspects of the 40–50 day oscillation in length-of-day and atmospheric angular momentum. *J. Geophys. Res.* **96**, 22643–22658.
- Dickey, J. O., Marcus, S. L. and Hide, R. 1992. Global propagation of interannual fluctuations in atmospheric angular momentum. *Nature* **357**, 484–488.
- Eubanks, T. M., Steppe, J. A., Dickey, J. O. and Callahan, P. S. 1985. A spectral analysis of the Earth's angular momentum budget. *J. Geophys. Res.* **90**, 5385–5404.
- Ghil, M. and Mo, K. 1991a. Intraseasonal oscillations in the global atmosphere. Part I: Northern Hemisphere and Tropics. *J. Atmos. Sci.* **48**, 752–779.
- Ghil, M. and Mo, K. 1991b. Intraseasonal oscillations in the global atmosphere. Part II: Southern Hemisphere. *J. Atmos. Sci.* **48**, 780–790.
- Gill, A. E. 1980. Some simple solutions for heat-induced tropical circulation. *Quart. J. R. Met. Soc.* **106**, 447–462.
- Gordon, C. T. and Stern, W. F. 1982. A description of the GFDL global spectral model. *Mon. Wea. Rev.* **110**, 625–644.
- Gutzler, D. S. and Ponte, R. M. 1990. Exchange of momentum among atmosphere, ocean, and solid earth associated with the Madden-Julian Oscillation. *J. Geophys. Res.* **95**, 18679–18686.
- Gutzler, D. S. and Madden, R. A. 1993. Seasonal variations of the 40–50 day oscillation in atmospheric angular momentum. *J. Atmos. Sci.* **50**, 850–860.

- Hayashi, Y. Y. and Sumi, A. 1986. The 30–40 day oscillations simulated in an “aqua planet” model. *J. Met. Soc. Japan* **64**, 451–466.
- Held, I. M. and Phillipps, P. J. 1987. Linear and non-linear barotropic decay on the sphere. *J. Atmos. Sci.* **44**, 200–207.
- Hide, R. and Dickey, J. O. 1991. Earth’s variable rotation. *Science* **253**, 629–637.
- Holton, J. R. 1992. *An introduction to dynamic meteorology*, 3rd edition. Academic Press, 511 pp.
- James, I. N. and James, P. M. 1989. Ultra-low-frequency variability in a simple atmospheric circulation model. *Nature* **342**, 53–55.
- James, I. N. and James, P. M. 1992. Spatial structure of ultra-low-frequency variability of the flow in a simple atmospheric circulation model. *Quart. J. Roy. Meteor. Soc.* **118**, 1211–1233.
- Kang, I. S. and Lau, K. M. 1990. Evolution of tropical circulation anomalies associated with 30–60 day oscillation of globally averaged angular momentum during northern summer. *J. Meteor. Soc. Japan* **68**, 237–249.
- Kidson, J. W. 1986. Index cycles in the Southern Hemisphere during the Global Weather experiment. *Mon. Wea. Rev.* **114**, 1654–1663.
- Kidson, J. W. 1988. Indices of the Southern Hemisphere zonal wind. *J. Climate* **1**, 183–194.
- Knutson, T. R. and Weickmann, K. M. 1987. 30–60 day atmospheric oscillations: Composite life cycles of convection and circulation anomalies. *Mon. Wea. Rev.* **115**, 1407–1436.
- Kutzbach, J. 1967. Empirical eigenvectors of sea level pressure, surface temperature, and precipitation complexes over North America. *J. Appl. Meteor.* **6**, 791–802.
- Lau, K. M. and Chan, P. H. 1985. Aspects of the 40–50 day oscillation during the northern winter as inferred from outgoing longwave radiation. *Mon. Wea. Rev.* **113**, 1889–1909.
- Lau, K. M., Kang, I. S. and Sheu, P. J. 1989. Principal modes of intraseasonal variations in atmospheric angular momentum and tropical convection. *J. Geophys. Res.* **94**, 6319–6332.
- Lau, K. M. and Phillips, T. J. 1986. Coherent fluctuations of extratropical geopotential height and tropical convection in intraseasonal time scales. *J. Atmos. Sci.* **43**, 1164–1181.
- Lau, N. C. and Lau, K. M. 1986. The structure and propagation of intraseasonal oscillations appearing in a GFDL general circulation model. *J. Atmos. Sci.* **43**, 2023–2047.
- Leith, C. E. 1973. The standard error of time-average estimates of climatic means. *J. Appl. Meteor.* **12**, 1066–1069.
- Lorenc, A. C. 1984. The evolution of planetary scale 200 mb divergent flow during the FGGE year. *Quart. J. Roy. Meteor. Soc.* **110**, 427–441.
- Madden, R. A. 1976. Estimates of the naturally occurring variability of time-averaged sea-level pressure. *Mon. Wea. Rev.* **104**, 942–952.
- Madden, R. A. 1981. A quantitative approach to long-range prediction. *J. Geophys. Res.* **86**, 9817–9825.
- Madden, R. A. 1987. Relationships between changes in the length of day and the 40 to 50 day oscillation in the tropics. *J. Geophys. Res.* **92**, 8391–8399.
- Madden, R. A. 1988. Large intraseasonal variations in wind stress over the tropical Pacific. *J. Geophys. Res.* **93**, 5333–5340.
- Madden, R. A. and Julian, P. 1971. Detection of a 40–50 day oscillation in the zonal wind. *J. Atmos. Sci.* **28**, 702–708.
- Madden, R. A. and Julian, P. 1972. Description of global scale circulation cells in the tropics with a 40–50 days period. *J. Atmos. Sci.* **29**, 1109–1123.
- Madden, R. A. and Shea, D. J. 1978. Estimates of natural variability of time-averaged temperatures over the United States. *Mon. Wea. Rev.* **106**, 1695–1703.
- Mitchell, J. M. 1976. An overview of climatic variability and its causal mechanisms. *Quart. Res.* **6**, 481–493.
- North, G. R., Bell, T. L., Cahalan, R. F. and Moeng, F. J. 1982. Sampling errors in the estimation of empirical orthogonal functions. *Mon. Wea. Rev.* **110**, 699–706.
- Robinson, W. A. 1991. The dynamics of the zonal index in a simple model of the atmosphere. *Tellus* **43A**, 295–305.
- Robinson, W. A. 1993. The generation of ultra-low-frequency variations in a simple global model. *J. Atmos. Sci.* **50**, 138–143.
- Rogers, J. C. and Van Loon, H. 1982. Spatial variability of sea level pressure and 500 mb height anomalies over the Southern Hemisphere. *Mon. Wea. Rev.* **110**, 1375–1392.
- Rosen, R. D. and Salstein, D. A. 1983. Variations in atmospheric angular momentum on global and regional scales and the length of day. *J. Geophys. Res.* **88**, 5451–5470.
- Rosen, R. D., Salstein, D. A. and Wood, T. M. 1991. Zonal contributions to global momentum variations on intraseasonal through interannual time scales. *J. Geophys. Res.* **96**, 5145–5151.
- Rossby, C. G. 1939. Relations between variations in the intensity of the zonal circulation of the atmosphere and the displacements of the semipermanent centers of action. *J. Mar. Res.* **2**, 38–55.
- Ting, M. and Lau, N. C. 1993. A diagnostic and modeling study of the monthly mean wintertime anomalies appearing in a 100-year GCM experiment. *J. Atmos. Sci.* **50**, 2845–2867.
- Trenberth, K. E. 1979. Interannual variability of the 500 mb zonal mean flow in the Southern Hemisphere. *Mon. Wea. Rev.* **107**, 1515–1524.
- Trenberth, K. E. 1984. Some effects of finite sample size and persistence on meteorological statistics. Part II: Potential Predictability. *Mon. Wea. Rev.* **112**, 2369–2379.

- Trenberth, K. E. 1985. Potential predictability of geopotential heights over the Southern Hemisphere. *Mon. Wea. Rev.* **113**, 54–64.
- Trenberth, K. E. and Christy, 1985. Global fluctuations in the distribution of atmospheric mass. *J. Geophys. Res.* **90**, 8042–8052.
- Van Loon, H. and Rogers, J. C. 1978. The seesaw in winter temperatures between Greenland and northern Europe. Part I: General description. *Mon. Wea. Rev.* **106**, 296–310.
- Von Storch, H. and Xu, J. S. 1990. Principal oscillation pattern analysis of the tropical 30- to 60-day oscillation. Part I: Definition of an index and its prediction. *Clim. Dyn.* **4**, 175–190.
- Walker, G. T. and Bliss, E. W. 1932. World Weather V. *Mem. Roy. Met. Soc.* **4**, 53–84.
- Wallace, J. M. and Gutzler, D. S. 1981. Teleconnections in the geopotential height field during the Northern Hemisphere winter. *Mon. Wea. Rev.* **109**, 784–812.
- Wallace, J. M. and Hsu, H. H. 1985. Another look at the index cycle. *Tellus* **37A**, 478–486.
- Weickmann, K. M., Lussy, G. R. and Kutzbach, J. E. 1985. Intraseasonal (30–60 day) fluctuations of outgoing long wave radiation and 250 mb streamfunction during northern winter. *Mon. Wea. Rev.* **113**, 941–961.
- Weickmann, K. M., Khalsa, S. J. S. and Eischeid, J. 1993. The atmospheric angular momentum cycle during the tropical Madden–Julian oscillation. *Mon. Wea. Rev.* **120**, 2252–2263.
- Zwiers, F. W. 1987. A potential predictability study conducted with an atmospheric general circulation model. *Mon. Wea. Rev.* **115**, 2957–2974.